

DOI: 10.1002/ (adfm.202006076)

## Full Papers

### A General Synthetic Strategy Towards Highly Doped Pyridinic Nitrogen-Rich Carbons

Xiaoling Mou, Jiabin Ma, Shuanghao Zheng, Xingkun Chen, Frank Krumeich, Roland Hauert, Ronghe Lin,\* Zhong-Shuai Wu,\* and Yunjie Ding\*

Dr. X. Mou, Dr. X. Chen, Prof. R. Lin, Prof. Y. Ding

Hangzhou Institute of Advanced studies, Zhejiang Normal University, Gengwen Road 1108,  
311231 Hangzhou, China

E-mail: catalysis.lin@zjnu.edu.cn

J. Ma, Dr. S. Zheng, Prof. Z-S. Wu, Prof. Y. Ding

State Key Laboratory of Catalysis

Dalian Institute of Chemical Physics, Chinese Academy of Sciences

Zhongshan Road 457, 116023 Dalian, China

E-mails: wuzs@dicp.ac.cn, dyj@dicp.ac.cn

Dr. F. Krumeich

Institute for Chemical and Bioengineering, Department of Chemistry and Applied Biosciences,  
ETH Zurich, Vladimir-Prelog-Weg 1, 8093 Zurich, Switzerland

Dr. R. Hauert

Swiss Federal Laboratories for Materials Science and Technology, EMPA, Überlandstrasse  
129, 8600 Dübendorf, Switzerland

J. Ma

University of Chinese Academy of Sciences

Yuquan Road 19A, Shijingshan District, Beijing 100049, China

Dr. S. Zheng, Prof. Z-S. Wu, Prof. Y. Ding

Dalian National Laboratory for Clean Energy,

Dalian Institute of Chemical Physics, Chinese Academy of Sciences,

Zhongshan Road 457, 116023 Dalian, China

**Keywords:** polymer, nitrogen-doped carbon, synthetic strategy, catalysis, lithium ion battery

Doping carbon materials with p-block elements such as nitrogen is an effective approach to tune electronic properties of the framework and can endow the hosts new characters. To date, highly doped carbons with tunable nitrogen speciation are still less explored due to the grand challenge in fabrication, *e.g.*, the typical synthesis based on pyrolysis of nitrogen-containing precursors shows a trade-off between the total nitrogen content and the carbonization temperature, limiting the value to *ca.* 12 wt.% at 1073 K. Herein, intensifying ring opening of cross-linked polymers through controlled pre-oxidation followed by conventional pyrolysis is

demonstrated as an elegant method to circumvent this challenge. In addition to fine tunability at different nitrogen speciation, this strategy can increase the nitrogen content by a 2-3-fold (maximum  $\approx 22$  wt.%) and shows general viability in six different N-bearing (co)polymers. The highly doped pyridinic nitrogen-rich carbons show *i*) a remarkable capacity of 879 mAh g<sup>-1</sup> at 0.1 A g<sup>-1</sup> and excellent cycling performance in lithium ion batteries, and *ii*) significantly boosted catalytic performance in the selective oxidation of diverse substrates. Therefore, this facile synthetic strategy and the tunability at nitrogen functionalities will greatly broaden the applications this new class of functional materials.

## 1. Introduction

Introducing foreign atoms into carbon framework is a general approach to tune the electronic and spin structure *via* the creation of vacancies or defects.<sup>[1-3]</sup> Among various dopants, nitrogen is most extensively studied, and thereby the N-doped carbon (NC) ensembles have showed promising prospects in numerous fields including CO<sub>2</sub> capture,<sup>[4-6]</sup> metal ion batteries,<sup>[7-9]</sup> electro-<sup>[10-12]</sup> and thermal-catalysis,<sup>[13-15]</sup> *etc.* For these materials, the total nitrogen content and the bonding configurations in a given carbon matrix can be viewed as the two key factors that largely determine the properties and performance of the hybrids. Systematic control over these two characters would allow the establishment of structure-performance relationships and ultimately of design rules of more advanced materials for targeted applications. In this context, several distinct strategies have been proposed to enrich the specific type of nitrogen species, such as pyridinic<sup>[9, 16-21]</sup> or quaternary nitrogen.<sup>[22, 23]</sup> However, the total N concentrations, in such cases, are usually relatively low, plus the synthesis is always limited to a very specific approach. To the best of our knowledge, a generalized synthetic protocol affording simultaneously a high nitrogen content (up to 22 wt.% in bulk) and delicate tuning of the nitrogen speciation has not been reported yet.

Carbonization of N-containing polymers is widely used as an effective approach to fabricate NCs.<sup>[24,25]</sup> Such derived materials, however, frequently show a decreased nitrogen content at elevated carbonization temperature. For instance, the polymers pyrolyzed at 1073 K possess around 12 wt.% N that is much lower than those of the precursors.<sup>[26]</sup> In addition, as quaternary N is favored at high temperatures owing to the higher thermostability, the conventional treatment offers limited control of the different nitrogen functionalities, particularly for highly doped carbons. Since all the nitrogen functionalities of NCs are evolved from the analogues of the polymer precursors, tuning the relative nitrogen speciation of the polymers before pyrolysis might impose alteration of nitrogen functionalities in the descendant. Earlier studies showed that heating polyaniline (PAni) at low temperatures ( $\leq 473$  K) in air or in vacuum leads to cross-linking of the polymer mainly through the formation of the Ph-NH-Ph structure (Ph = phenazine ring).<sup>[27]</sup> This ensemble was suggested as the precursor of the pyrrolic and quaternary nitrogen (N5 and N3) on the basis of detailed  $^{15}\text{N}$  NMR experiments.<sup>[28]</sup> On the contrary, the oxime or nitrile structures, likely derived from the quinoid unit of PAni by reconstruction of the polymer backbone, can only be detected at high carbonization temperatures ( $> 673$  K),<sup>[29]</sup> and the imine N associated with the quinoid unit might eventually transform into pyridinic nitrogen (N6). Following these inspiring works, we intended to *i*) develop a method to moderate the different nitrogen configurations in the polymer, *ii*) further examine the impact on the nitrogen speciation of the yielded carbons, and *iii*) extend the scope to other polymeric materials.

Herein, we report a facile strategy to synthesize a family of highly N-doped carbons with tunable nitrogen functionalities by intensifying ring-opening of cross-linked polymer precursors through controlled pre-oxidation in flowing air, followed by conventional carbonization in inert stream (**Figure 1**). More importantly, the developed method is also effective when extrapolated to a total of six types of

(co)polymers synthesized from the respective monomers with different nature. The impacts of pre-oxidation treatment on the nitrogen speciation, composition, structure, and morphology of the finally yielded NCs were systematically studied by coupling a spectrum of characterization techniques. Finally, we demonstrated the superiority of the highly N-doped carbons with enriched pyridinic nitrogen speciation as a new class of advanced functional materials in lithium ion batteries (LIBs) and in diverse catalytic applications, including the selective oxidation of different aromatic hydrocarbons and benzylic alcohols.

## 2. Results and Discussion

Our approach for the synthesis of highly N-doped carbons comprises the controlled peroxidation of a polymer precursor and a subsequent pyrolysis step. To demonstrate the broad applicability of this strategy, a total of six different polymers including three polyaniline-based polymers, *i.e.*, PANi, polyaniline-polypyrrol copolymer (PANiPy), and polyaniline-phytic acid complex (PANiPA), two polypyrroles (PPy and PPy-s) derived from different synthetic methods, and an additional polydopamine polymer (PDA), was targeted. Controlled oxidation of the polymers was mainly studied at 393-673 K as further increasing the temperature to 723 K led to significant combustion and very low yield of the carbonized sample (**Figure S1**), and thus was not discussed hereafter.

### 2.1. Moderation of nitrogen functionalities of polymer precursors

First, diffuse reflectance infrared Fourier transform spectroscopy (DRIFT) was employed to examine the variation of different functionalities of the polymers upon oxidation treatment. As a representative, **Figure 2a** shows the spectra of the PANiPy- $T_1$  ( $T_1$  = pre-oxidation temperature in K) series. With the increasing oxidation temperature, most of the bands showed weakened intensities, including the C-H vibrations at 904, 1100, 2850, and 2920  $\text{cm}^{-1}$ ,

two aniline oligomer-related vibrations at 695 and 756  $\text{cm}^{-1}$ , and that of  $\text{HSO}_4^-/\text{SO}_3^-$  on sulfonated aromatic ring at 1033  $\text{cm}^{-1}$ . In addition, the band at 1235  $\text{cm}^{-1}$  that can be ascribed to  $\nu(\text{C-N})$  in the N,N'-diphenyl-1,4-phenylenediamine unit almost completely vanished at 573 K. Meanwhile, a new band at 2220  $\text{cm}^{-1}$ , which was tentatively assigned to the nitrile ( $\text{C}\equiv\text{N}$ ) or oxime ( $\text{N}=\text{C}=\text{O}$ ) vibrations,<sup>[30,31]</sup> was already found at 523 K and the intensity increased with the pre-oxidation temperature. In stark contrast, this band showed much lower intensity in the polymer even after treated at 673 K in  $\text{N}_2$  (**Figure S2**). Another two polymers (PAni and PPy-s) subject to treatment in the different atmospheres were then checked, and similar observations were also found in both series despite the very different compositions (**Figure S2**). These results suggested that, in comparison to the conventional direct carbonization wherein crosslinking of polymer chains is dominant in low temperature (<673 K),<sup>[28,30]</sup> the controlled oxidation treatment is a more disruptive manner even under milder conditions and thus promotes the formation of nitrile or oxime structures through ring opening in the polymers.

To gain more insight on the variations of different functionalities upon pre-treatment, the evolution of volatile species on the PAniPy- $T_1$  series was followed by thermogravimetric analysis coupled with mass spectroscopy (TGA-MS, **Figures 2b** and **S3**). The PAniPy-393 showed a weight loss of *ca.* 50 wt.% upon 1273 K in Ar, accompanied with two distinct slopes: the low-temperature region at around 523 K is mainly associated with the release of  $\text{NH}_3$  with relatively small contributions of HCN,  $\text{H}_2\text{O}$ , and  $\text{SO}_2$ , and the high-temperature region around 973 K is due to the development of both HCN and  $\text{NH}_3$ . The release of  $\text{CO}_x$  and NO was very weak in Ar, which was different from the case when running in  $\text{O}_2$ . The PAniPy-673 was then checked and its TG curve showed a similar weight loss of *ca.* 50 wt.% up to 1273 K, but with only one slope at the high-temperature around 973 K. The disappearance of the low-temperature weight loss suggests that pre-oxidation treatment at 673 K should be sufficient to partially release  $\text{NH}_3$ . In comparison to the PAniPy-393, this

pre-treated sample shows prominent differences in the respective MS fragments. At first, the  $\text{NH}_3$  signal became much weaker in PAniPy-673, whereas the HCN release was significantly promoted. Second, more CO was evolved and the peak was shifted to the high-temperature region. To verify whether such features are only associated with the copolymer, the PAni- $T_1$  series was also examined. Indeed, similar trends were observed on PAni-673, showing significantly enhanced releases of HCN and CO, and dramatically decreased amounts of  $\text{NH}_3$  and  $\text{CO}_2$  (**Figure S4**). To better depict the evolution of different nitrogen speciation, the relative contribution of HCN and  $\text{NH}_3$  was estimated by comparing the  $S_{\text{HCN}}:S_{\text{NH}_3}$  values of the polymers oxidized at 393 and 673 K, where  $S$  is the integration of respective fragment in the MS. For the PAniPy- $T_1$  series, these values are 0.8 (393 K) and 22.9 (673 K), and for the PAni- $T_1$  series, 0.4 (393 K) and 8.0 (673 K). The above findings clearly demonstrate that controlled oxidation is effective in moderating the relative contribution of different nitrogen functionalities of the polymers. By combining the DRIFT and TGA-MS results, it is further confirmed that the enhanced evolutions of HCN and CO, which are quite overlapping, might originate from the nitrile or oxime ensembles.

## 2.2. Speciation of nitrogen-doped carbons

The polymers after pre-treatment at different temperatures were further converted to NC by carbonization in Ar at 1073 K. The C, N, and H contents of the polymers and the corresponding NCs were determined by elemental analysis (**Figure 3a**). Interestingly, the total nitrogen content can be increased to different extents with the pre-oxidation treatment, irrespective of the different polymers. The developed approach is most effective to the polyaniline-based polymers, *i.e.*, PAni, PAniPy, and PAniPA, for which the nitrogen content can be increased by 2-3 times, whereas the changes are relatively milder for the rest three polymers ( $<1.6$  times). In addition, the maximal nitrogen content strongly depends on the pre-oxidation temperature. For most of the polymers it appeared at 673 K but shifted to 623 K for the PAniPA and PPy.

Thus, the compositional and structural differences highlight the need of individual optimization of this parameter for different polymers. The dependence of the nitrogen content as a function of the carbonization temperature (1073-1273 K) was then examined on the PANi- $T_1$  series (**Figure S5**). With elevated temperatures, however, the nitrogen content showed significant loss and the pre-oxidation effect became less prominent, probably because of the intrinsic instability of the nitrogen functionalities under such harsh pyrolysis conditions.

X-ray spectroscopy (XPS) was then performed to study the variations of different nitrogen speciation in NC after different pre-treatments. First, we compared the N 1s XPS spectra of the corresponding NCs derived for the PANiPy, PANi, and PPy with pre-oxidation at 393 and 673 K (**Figure S6**). Typical two adjacent peaks at 396-404 eV binding energy (*B.E.*) can be found for all the samples, and in general, the contribution of the peak at low *B.E.* increased for all the samples pre-oxidized at higher temperatures, hinting similar trends in nitrogen speciation variation. To further elucidate this point, deconvolution was conducted for the whole PANiPy- $T_1$ -1073 series (**Figure 3b** and **Table S1**). In line with the earlier studies,<sup>[26]</sup> the presence of all the four kinds of nitrogen speciation was confirmed in all those samples, with N6, N5, and N3 as the major constituents. With increasing the pre-treatment temperature, N6 steadily developed and the share reached from 24.0% to 42.3% while N3 showed an opposing trend, with the share decreased from 33.1% to 23.7%, as well as the N0. Besides, the share of N5 stayed relatively stable and did not show any clear dependence on the temperature variable.

The significant alterations in the total nitrogen content and the distribution of different speciation could be linked to the variations of nitrogen functionalities induced by the pre-oxidation treatment. TGA-MS analysis revealed that, instead of  $\text{NH}_3$ , HCN was the main N-containing species evolved during carbonization of the polymers pre-treated at 673 K, plus the release of a larger amount of  $\text{CO}_x$ . This would therefore lead to more

carbon removed from the framework and a higher N:C ratio of the resulting NCs. On the other hand, the increased share of N6 speciation might be probably related to the favorable formation of nitrile and/or oxime ensembles as supported by both DRIFT and TGA-MS. In fact, these architectures are the derivatives of imines that have been proposed as the precursors to N6 speciation.<sup>[28,29]</sup>

## 2.2. Structural and morphological evolution

The structural variations, induced by the pre-treatment, of the N-doped carbons from different polymers were studied by N<sub>2</sub> sorption. The total surface area of the corresponding NCs as a function of  $T_1$  is presented in **Figure 3c**. Volcano-like curves are observed for most of the samples with the maximal reached at 573-623 K, suggesting that mild oxidation of the polymers is most effective in the development of surface area and porosity, particularly the mesopores. The NCs from PAniPy are the only exception, for which the influence is marginal likely due to the special hollow nanosphere morphology (*vide infra*). The morphologies of selected NCs derived from the two polyaniline-based polymers were examined by scanning electron microscopy (SEM, **Figure S7**), and showed a clear ‘memory effect’. The PAni- $T_1$ -1073 and PAniPA- $T_1$ -1073 series both showed a similar inter-connected granular morphology like the polymer precursors, while the PAniPy- $T_1$ -1073 series presented an inter-connected nanosphere morphology. The unique morphology of PAniPy- $T_1$ -1073 is a result of the simultaneous self-assembly of both aniline and pyrrole monomers around tergitol (surfactant), as has been discussed in an earlier study.<sup>[32]</sup> High-angle annular dark field scanning transmission electron microscopy (HAADF-STEM) analysis of this series further reveals that, different from the polymer precursor, the pyrolyzed samples display hollow morphology (**Figures 3d** and **S8**), which could be explained by the different thermal expansion coefficients of the two polymers. Furthermore, PAniPy-

623 showed relatively larger inner and outer diameters than PAniPy-393, hinting that high-temperature pre-treatment is favorable for the development of hollow structures.

### 2.3. Applications of highly doped carbons with rich pyridinic nitrogen

As a class of abundant and relatively cheap materials, nitrogen-doped carbons have been extensively explored in broad fields such as adsorbent, battery, supercapacitor, and catalysis. Despite the great versatility in diverse applications, the studies exploring the potential of highly doped carbons, especially when coupled with systematic alternation in specific nitrogen speciation, are scarcely reported. In this context, the materials developed in our work can provide a great chance for this task. Accordingly, the performances of the whole PAniPy- $T_1$ -1073 series as anode for lithium ion batteries and in the selective oxidation of aromatic hydrocarbons and benzylic alcohols were investigated. The PAniPy materials other than PAni and PAniPA was selected for applications based on two considerations: *i*) a wide range of nitrogen content (9-20 wt.%) should be covered, and *ii*) the similar morphology and porosity (**Table S2**) to exclude their impacts on Li ions storage and catalysis.

#### 2.3.1. Electrochemical performance for LIBs

We first tested the electrochemical performance of PAniPy-673-1073 in the voltage range of 0.01-3.0 V vs.  $\text{Li}^+/\text{Li}$ . In the first discharge cycle (**Figure S9a**), the typical cathodic peaks at 0.5-1.0 V were observed for PAniPy-673-1073, which was attributed to the formation of solid electrolyte interphase.<sup>[33]</sup> While the discharge peak at 1.66 V was likely caused by the irreversible reactions between Li ions and graphitic nitrogen in PAniPy-673-1073.<sup>[34]</sup> With the continuous cycling, the cathodic peaks disappeared, indicative of outstanding reversibility of PAniPy-673-1073 as anode for LIBs. Such phenomenon could also be observed from the change of the discharge plateau in GCD profiles (**Figure S9b**). With increasing the pre-oxidation temperature from 393 to 673

K, the capacities of PAniPy- $T_1$ -1073 materials were gradually enhanced from 451 mAh g<sup>-1</sup> for PAniPy-393-1073, 493 mAh g<sup>-1</sup> for PAniPy-523-1073, 549 mAh g<sup>-1</sup> for PAniPy-573-1073, 690 mAh g<sup>-1</sup> for PAniPy-623-1073 to the highest value of 879 mAh g<sup>-1</sup> for PAniPy-673-1073 (**Figure 4a**). The progressive improvement of the capacity was largely ascribed to the gradual increase of N-doped content in the PAniPy- $T_1$ -1073 series, especially for the pyridinic nitrogen with stronger adsorption ability of Li ion. Most importantly, PAniPy-673-1073 *via* pre-oxidation and carbonization process showed a higher capacity than most of the state-of-the-art N-doped carbon-based anodes for LIBs (**Table S3**), for instance, N-doped porous graphene (742 mAh g<sup>-1</sup>),<sup>[35]</sup> N-doped graphene sheets (832.4 mAh g<sup>-1</sup>),<sup>[34]</sup> N-doped carbon spheres (666 mAh g<sup>-1</sup>),<sup>[36]</sup> demonstrating that the developed pre-oxidation and carbonization polymer method is a feasible strategy to introduce more electronegative N-heteroatom with high doping level in carbon-based materials, catering for notably improved electrochemical performance for Li ion storage. Furthermore, albeit possessing the lowest specific surface area (87 m<sup>2</sup> g<sup>-1</sup>) in PAni- $T$ -1073 anodes, the PAni-673-1073 exhibited the most abundant nitrogen content (22.0%) and delivered the highest capacity of 634 mAh g<sup>-1</sup> at 0.1 A g<sup>-1</sup> (**Figure S9**), much higher than PAni-393-1073 (508 mAh g<sup>-1</sup>), PAni-523-1073 (574 mAh g<sup>-1</sup>), PAni-573-1073 (582 mAh g<sup>-1</sup>), and PAni-623-1073 (527 mAh g<sup>-1</sup>). It strongly suggests that the high nitrogen level plays a more important role in improving capacity other than large specific surface area. However, the capacity of PAni-673-1073 (634 mAh g<sup>-1</sup>) was still inferior to that of PAniPy-673-1073 (879 mAh g<sup>-1</sup>), due to the agglomerate bulks of PAni under higher pre-oxidation temperature. In addition, the PAniPy-673-1073 electrode showed reversible capacity of 685 mAh g<sup>-1</sup> at 0.2 A g<sup>-1</sup> in the 50<sup>th</sup> cycle (**Figure 4b**), which is approximately two times higher than that of PAniPy-393-1073 (348.3 mAh g<sup>-1</sup>), strongly suggestive of robust lithium storage performance of PAniPy-673-1073 in term of high capacity and long lifespan.

Remarkably, the PAniPy-673-1073 still exhibited satisfactory capacity of 301 mAh g<sup>-1</sup> even at a high current density of 5 A g<sup>-1</sup> (**Figures 4c** and **S10c**), and a reversible capacity of PAniPy-673-1073 with *ca.* 725 mAh g<sup>-1</sup> was regained when the current density was suddenly switched to 0.1 A g<sup>-1</sup>. The excellent rate capability of PAniPy-673-1073 is strongly related to the fast charge transfer process, proved by the EIS of PAniPy-673-1073 with lower semicircle ( $R_{ct} = 34.6 \Omega$ ) in the high frequency region (**Figure 4d**). Furthermore, the long-term cycle life of PAniPy-673-1073 was demonstrated for 400 continuous charge-discharge cycles at 2 A g<sup>-1</sup> with a tiny average capacity loss of only 0.078% per cycle, and an outstanding CE of more than 99.8% (**Figure S10d**).

### 2.3.2. Selective oxidations

Distinct features can be observed over the PAniPy-*T*<sub>1</sub>-1073 series in the selective oxidation of benzyl alcohol (**Figure 5a**). First, the conversion level showed a volcano-like curve dependence on the pre-treatment temperature, and at 623 K it reached the maximal that is 2-fold higher than that of conventional PAniPy-393-1073. Second, the selectivity of benzoic acid, the deep oxidation product, increased steadily (from 33% to 80%) at the compensation of benzaldehyde with the rising pre-treatment temperature. Replacing air with O<sub>2</sub> gives excellent yield of benzoic acid (99%) over the best-performed PAniPy-623-1073, which is remarkable among the metal-free carbon-based catalysts (**Table S4**). When evaluated in toluene oxidation (**Figure 5b**), a similar activity trend was observed as in the oxidation of benzyl alcohol, with the maximal of 1.7-fold increase in conversion level for PAniPy-623-1073. Besides, the selectivity of benzoic acid, the major product over the whole series, also increased (from 69% to 93%), and more importantly the side-reactions were largely prohibited (total byproduct selectivity decreased from 21% to 2%). To verify if the above phenomenon were only

associated with the specific substrates, two additional substrates (cinnamyl alcohol and ethylbenzene) were also studied (**Figure S11**). Like in the toluene oxidation, PAniPy-623-1073 showed >2-fold increase in activity (from 36% to 74%) and acetophenone selectivity (from 37% to 87%), with significantly reduced byproduct selectivity (from 51% to 0.6%). For cinnamyl alcohol, a more challenging substrate, PAniPy-673-1073 was the best-performing catalyst, showing 1.3-fold activity increase in comparison to PAniPy-393-1073. Notably, it can also promote the formation of cinnamic acid that is not detected on PAniPy-393-1073. These results demonstrated that the highly nitrogen-doped carbons can not only significantly boost the catalytic activity but also moderate the reaction path and product distribution, thus might open up more possibilities in other applications.

### 2.3.3. Structure-performance relationships

To shed light on the distinct behaviors of the highly N-doped carbon, tentative correlations between the electrochemical and catalytic activity and the total and respective nitrogen speciation were made in order to establish the structure-performance relationships (**Figure 6**). Since the share of N3 species stayed relatively stable in this series while the N0 sites are in minor percentage on the basis of XPS, these speciations were not further considered. Interestingly, the capacity in LIBs increased almost linearly with the total nitrogen as well as the share of N6 sites. As compared with carbon atoms, the high doping content of nitrogen with higher electronegativity is much beneficial to the formation of a robust bonding to Li ions, leading to the remarkable enhancement of capacity with the N content increased. Furthermore, the defects created by the heteroatoms, especially for the pyridinic-N and pyrrolic-N,<sup>[35]</sup> are able to serve as a significant role in accommodating or adsorbing Li ions, further contributing to the improvement of Li ion storage. In catalysis, the

correlations of benzoic acid yield as a function of the total nitrogen, and the shares of N6 and N3 sites showed volcano-like dependency. The promotional effect of high nitrogen content is evidenced from the significantly boosted activity, particularly at 9-16 wt.%, albeit the activity slightly dropped at even higher nitrogen content. The latter suggested that the individual nitrogen speciation should also play a role in determining the performance. Indeed, the activity developed almost linearly with the increasing share of N6 species in a very wide range (22-37 at.%), strongly hinting its decisive contribution in the catalytic cycles. Further increasing the N6 share led to loss of activity, which might be caused by the sacrificing of the N3 functionalities.

### 3. Conclusion

In this work, we have developed a general strategy to fabricate a new family of highly doped carbon materials (up to 22 wt.% N) with tunable nitrogen speciation, and demonstrated the great versatility for a wide range of different (co)polymers. Combining controlled pre-oxidation treatment with conventional carbonization led to a 2-3 fold increase in total nitrogen content and the favored development of pyridinic N at the expense of quaternary N species. These can be rationalized by the alternation of nitrogen functionalities upon oxidation of the polymers, as multiple characterization techniques revealed the favorable formation of nitrile or oxime ensembles, hinting the intensified ring-opening of cross-linked polymers under oxidative ambience. Furthermore, these novel functional materials show distinct behaviors in electrochemical cell and catalysis, differing markedly from those of conventional N-doped carbons. The developed highly doped pyridinic nitrogen-rich carbons show a remarkable capacity of 879 mAh g<sup>-1</sup> at 0.2 A g<sup>-1</sup> and excellent cycling performance in LIBs, and significantly boosted activity and altered product distribution in the selective oxidation of diverse aromatic hydrocarbons and benzylic alcohols. Finally, given the great versatility of our synthetic strategy and the broad applications of metal-free carbon materials, we anticipate that

our study will also have implications for future studies in other catalysis, batteries, and supercapacitors, wherein the tunable nitrogen speciation of these materials provides an excellent chance to establish the material design rules.

## 4. Experimental Section

### 4.1. Material synthesis

The polyaniline-polypyrrole copolymer (denoted as PAniPy) was synthesized following a previously established protocol<sup>28</sup> with a few modifications. A mixture of tergitol (92.4 mg, Sigma-Aldrich, type 15-S-9), aniline (50 mmol, Acros, 99.5%), and pyrrole (50 mmol, Sigma-Aldrich, 98%) was dissolved in 160 cm<sup>3</sup> deionized water, and stirred at 500 rpm in an ice bath for 30 min. Another solution of ammonium persulfate (4.56 g, Acros Organics, 98%, dissolved in 40 cm<sup>3</sup> deionized water) was prepared, cooled at ice bath for 30 min, and added dropwise into the above solution under vigorous stirring. Afterwards, stirring was continued in the ice bath for another 1 h, and the polymerization was continued for another 23 h at room temperature. The yielded solid was filtrated, washed with deionized water, and dried at 373 K overnight.

The synthesis of polyaniline (PAni),<sup>[26]</sup> polypyrrole (PPy),<sup>[6]</sup> polydopamine (PDA),<sup>[37]</sup> and the polyaniline-phytic acid complex (PAniPA)<sup>[38]</sup> was conducted following the respective procedures reported in the earlier literature, and was detailed in the **Supporting Information**. An additional type of polypyrrole (PPy-s) was also prepared following the synthetic protocol of PAniPy but in the absence of aniline.

The as-prepared polymers were further converted to corresponding N-doped carbons in a tubular oven by the following two steps: firstly pre-oxidized in flowing air at different temperatures ( $T_1$ , 393, 523, 573, 623, 673 K, 2 K min<sup>-1</sup>, 3 h), and then further carbonized in flowing N<sub>2</sub> at a higher temperature (1073 K, if not otherwise specified).

#### 4.2. Characterization methods

Elemental analysis of C, H, N, and O was determined by infrared spectroscopy using a LECO TruSpec Micro and a LECO 628 O Micro combustion furnace, respectively. Nitrogen adsorption and desorption isotherms were recorded using a Micromeritics TriStar analyser instrument. Prior to analysis, samples were degassed overnight at 393 K. Diffuse reflectance infrared Fourier transform spectroscopy (DRIFTS) were recorded on a Bruker Vertex 400 spectrometer equipped with liquid N<sub>2</sub> cooled MCT detector and a Harrick diffuse reflection accessory (4000-700 cm<sup>-1</sup>, 4 cm<sup>-1</sup> resolution, 32 scans). Prior to analysis, samples were degassed in Ar (20 cm<sup>3</sup> min<sup>-1</sup>) for 1 h. Thermogravimetric analysis (TGA) was performed in a Mettler Toledo TGA/DSC 1 Star system connected to a Pfeiffer Vacuum Thermo-Star GDS 320 T1 mass spectrometer (MS). The program involved dehydrating the samples at 373 K in flowing air followed by ramping the temperature from 373-1073 K at a rate of 10 K min<sup>-1</sup> all under argon or flowing air (100 cm<sup>3</sup> min<sup>-1</sup>). The fragments with *m/e* of 18, 28 and 44 were followed by MS indicative of H<sub>2</sub>O, CO and CO<sub>2</sub>, respectively. X-ray photoelectron spectroscopy (XPS) was measured in a Physical Electronics Quantum 2000 X-ray photoelectron spectrometer using monochromatic Al-K $\alpha$  radiation, generated from an electron beam operated at 15 kV, and equipped with a hemispherical capacitor electron-energy analyzer. The solids were analyzed at the electron take-off angle of 45° and the pass energy of 46.95 eV. The spectrometer was calibrated for the Au 4f<sub>7/2</sub> signal to be at 84.0 ± 0.1 eV and had a resolution step width of 0.2 eV. The N 1s envelopes were fitted by mixed Gaussian-Lorentzian component profiles after Shirley background subtraction. The selected peak positions of the different nitrogen species were based on literature reported data and fixed with an error of ±0.2 eV. The elemental concentrations were quantified based on the measured photoelectron peak areas (C 1s and N 1s) after Shirley background subtraction, using PHI-MultiPak software and the built-in relative sensitivity factors, which were corrected for the system transmission function. Scanning electron microscopy (SEM) was

conducted on a Quanta 200F instrument operating at 10 kV and 50 pA. The powder sample was dispersed in dry form onto fresh carbon paint deposited on an aluminum holder and subsequently coated by a Pt-Pd alloy (*ca.* 10 nm thickness) to prevent charging. Scanning transmission electron (STEM) micrographs with a high-angle annular dark-field (HAADF) detector were acquired on a Talos F200X instrument (Thermos Fisher Scientific) operated at 200 kV.

#### **4.3. Electrochemical tests**

Lithium ion batteries were assembled at CR2016 coin cells using lithium foil as the counter and reference electrode, PANiPy-T-1073 electrode as working electrode, and commercial LB-113 as electrolyte. The working electrodes were prepared through the mixture of N-doped carbon powder, carbon black, and polyvinylidene fluoride with a weight ratio of 8:1:1 in N-methylpyrrolidone solvent. The resultant electrode slurry was pasted onto a copper current collector, followed by vacuum drying at 393 K for 12 h, and then cut into electrode plate with a diameter of 12 mm. The galvanostatic charge-discharge (GCD) profiles were operated at a LAND CT2001A battery tester in a voltage range from 0.01 to 3.0 V. Electrochemical impedance spectra (EIS) and cyclic voltammetry (CV) curves were carried out at a CHI 760E workstation. The CV tests were conducted at 0.01-3.0 V with a scanning rate of 0.1 mV s<sup>-1</sup>. The EIS data were collected at an ac amplitude of 5 mV with the frequency range from 100 to 0.1 Hz.

#### **4.4. Catalytic tests**

The selective oxidation of two benzylic alcohols (benzyl alcohol, 99.8%, Sigma-Aldrich, cinnamyl alcohol, Sigma-Aldrich, 98%) and two aromatic hydrocarbons (toluene, TCI, 99.5%, ethylbenzene, Acros Organics, 99.8%) was studied in pressure tube reactors ( $V = 21 \text{ cm}^3$ , Ace Glass) equipped with a magnetic stirrer and heated using an oil bath. In a typical experiment, the pre-dried catalyst (10 mg, 373 K, 12 h), and a solution of the substrate

(1 mmol) in deionized water (3 cm<sup>3</sup>) and tert-butyl hydroperoxide (TBHP, 3 cm<sup>3</sup>, Sigma-Aldrich, 70 wt.% in H<sub>2</sub>O) were added to the reactor. After replacing air with Ar three times, the reactor was sealed and heated to 373 K at autogenous pressure for 6 h. The reaction mixture was quenched with ice-water. After separation of the solid by centrifugation, the organics were extracted with cyclohexane (3 cm<sup>3</sup>, ABCR, 99%) and 0.01 cm<sup>3</sup> of the oil phase was added to 1 cm<sup>3</sup> acetonitrile (AcroSeal, 99.9%) for further analysis. Samples were analyzed using an Agilent 1260 Infinity HPLC equipped with an Agilent Zorbax C18 column (150 x 3.0 mm, 3 μm, 298 K) and both DAD and RID detectors. The substrate and product concentrations were calibrated with reference to pure standards.

### Supporting Information

Supporting Information is available from the Wiley Online Library or from the author.

### Acknowledgements

This work was financially supported by the National Key R&D Program of China (Grants 2016YBF0100100, 2016YFA0200200), National Natural Science Foundation of China (Grants 51872283, 21805273), Liaoning BaiQianWan Talents Program, Natural Science Foundation of Liaoning Province, Joint Research Fund Liaoning-Shenyang National Laboratory for Materials Science (Grant 20180510038), LiaoNing Revitalization Talents Program (Grant XLYC1807153), DICP (DICP ZZBS201708, DICP ZZBS201802, DICP I202032), DNL Cooperation Fund, CAS (DNL180310, DNL180308, DNL201912, and DNL201915), DICP&QIBEBT (Grant DICP&QIBEBT UN201702). We thank Drs. A. Martin and J. Zhang for the assistance with SEM. ScopeM of ETH Zurich is acknowledged for the use of their facilities. X. Mou, J. Ma, and S. Zheng contributed equally to this work.

Received: ((will be filled in by the editorial staff))

Revised: ((will be filled in by the editorial staff))

Published online: ((will be filled in by the editorial staff))

### References

- [1] X. Liu and L. Dai, *Nat. Rev. Mater.*, 2016, **1**, 1-12.
- [2] L. He, F. Weniger, H. Neumann and M. Beller, *Angew. Chem. Int. Ed.*, 2016, **55**, 12582-12594.
- [3] X.-K. Kong, C.-L. Chen and Q.-W. Chen, *Chem. Soc. Rev.*, 2014, **43**, 2841-2857.

- [4] J. W. F. To, J. J. He, J. G. Mei, R. Haghpanah, Z. Chen, T. Kurosawa, S. C. Chen, W. G. Bae, L. J. Pan, J. B. H. Tok, J. Wilcox and Z. N. Bao, *J. Am. Chem. Soc.*, 2016, **138**, 1001-1009.
- [5] J. J. He, J. W. F. To, P. C. Psarras, H. P. Yan, T. Atkinson, R. T. Holmes, D. Nordlund, Z. N. Bao and J. Wilcox, *Adv. Energ. Mater.*, 2016, **6**, 1502491.
- [6] M. Sevilla, P. Valle - Vigón and A. B. Fuertes, *Adv. Funct. Mater.*, 2011, **21**, 2781-2787.
- [7] W. Guo, X. Li, J. Xu, H. K. Liu, J. Ma and S. X. Dou, *Electrochim. Acta*, 2016, **188**, 414-420.
- [8] X. Li, J. Liu, Y. Zhang, Y. Li, H. Liu, X. Meng, J. Yang, D. Geng, D. Wang and R. Li, *J. Power Sources*, 2012, **197**, 238-245.
- [9] Y. Xie, Y. Chen, L. Liu, P. Tao, M. Fan, N. Xu, X. Shen and C. Yan, *Adv. Mater.*, 2017, **29**, 1702268.
- [10] N. Daems, X. Sheng, I. F. Vankelecom and P. P. Pescarmona, *J. Mater. Chem. A*, 2014, **2**, 4085-4110.
- [11] C. Hu and L. Dai, *Angew. Chem. Int. Ed.*, 2016, **55**, 11736-11758.
- [12] H. B. Yang, J. Miao, S.-F. Hung, J. Chen, H. B. Tao, X. Wang, L. Zhang, R. Chen, J. Gao and H. M. Chen, *Sci. Adv.*, 2016, **2**, e1501122.
- [13] K. Chizari, A. Deneuve, O. Ersen, I. Florea, Y. Liu, D. Edouard, I. Janowska, D. Begin and C. Pham - Huu, *ChemSusChem*, 2012, **5**, 102-108.
- [14] W. Qi and D. Su, *ACS Catal.*, 2014, **4**, 3212-3218.
- [15] D. S. Su, J. Zhang, B. Frank, A. Thomas, X. Wang, J. Paraknowitsch and R. Schlögl, *ChemSusChem*, 2010, **3**, 169-180.
- [16] W. Ding, Z. Wei, S. Chen, X. Qi, T. Yang, J. Hu, D. Wang, L. J. Wan, S. F. Alvi and L. Li, *Angew. Chem. Inter. Ed.*, 2013, **52**, 11755-11759.

- [17] B. He, F. Liu and S. Yan, *J. Mater. Chem. A*, 2017, **5**, 18064-18070.
- [18] M. S. Lee, H.-J. Choi, J.-B. Baek and D. W. Chang, *Appl. Energ.*, 2017, **195**, 1071-1078.
- [19] Z. Luo, S. Lim, Z. Tian, J. Shang, L. Lai, B. MacDonald, C. Fu, Z. Shen, T. Yu and J. Lin, *J. Mater. Chem.*, 2011, **21**, 8038-8044.
- [20] H. Miao, S. Li, Z. Wang, S. Sun, M. Kuang, Z. Liu and J. Yuan, *Int. J. Hydrog. Energ.*, 2017, **42**, 28298-28308.
- [21] J. Wu, L. Ma, R. M. Yadav, Y. Yang, X. Zhang, R. Vajtai, J. Lou and P. M. Ajayan, *ACS Appl. Mater. Inter.*, 2015, **7**, 14763-14769.
- [22] Y. Xia and R. Mokaya, *Chem. Mater.*, 2005, **17**, 1553-1560.
- [23] L. Zhang, Z. Su, F. Jiang, L. Yang, J. Qian, Y. Zhou, W. Li and M. Hong, *Nanoscale*, 2014, **6**, 6590-6602.
- [24] T. Z. Yang, T. Qian, M. F. Wang, X. W. Shen, N. Xu, Z. Z. Sun, C. L. Yan, *Adv. Mater.*, 2016, **28**, 539-545.
- [25] T. Z. Yang, M. F. Wang, J. Liu, J. Q. Zhou, Z. Z. Sun, M. Z. Chen, C. L. Yan, *J. Mater. Chem. A*, 2015, **3**, 6291-6296.
- [26] R. Lin, S. K. Kaiser, R. Hauert and J. Perez-Ramirez, *ACS Catal.*, 2018, **8**, 1114-1121.
- [27] M. Trchova, P. Matejka, J. Brodinova, A. Kalendova, J. Prokes and J. Stejskal, *Polym. Degrad. Stabil.*, 2006, **91**, 114-121.
- [28] S. Kuroki, Y. Hosaka and C. Yamauchi, *Carbon*, 2013, **55**, 160-167.
- [29] M. Trchova, E. N. Konyushenko, J. Stejskal, J. Kovarova and G. Ciric-Marjanovic, *Polym. Degrad. Stabil.*, 2009, **94**, 929-938.
- [30] Z. Rozlivkova, M. Trchova, M. Exnerova and J. Stejskal, *Synthetic Met.*, 2011, **161**, 1122-1129.
- [31] M. Trchová and J. Stejskal, *Pure Appl. Chem.*, 2011, **83**, 1803-1817.

- [32] C. Zhou, J. Han, G. Song and R. Guo, *J. Polym. Sci. Polym. Chem.*, 2008, **46**, 3563-3572.
- [33] X. Liu, J. Zhang, S. Guo and N. Pinna, *J Mater. Chem. A*, 2016, **4**, 1423-1431.
- [34] L. L. Tian, X. Y. Wei, Q. C. Zhuang, C. H. Jiang, C. Wu, G. Y. Ma, X. Zhao, Z. M. Zong and S. G. Sun, *Nanoscale*, 2014, **6**, 6075-6083.
- [35] Z.-Y. Sui, C. Wang, Q.-S. Yang, K. Shu, Y.-W. Liu, B.-H. Han and G. G. Wallace, *J Mater. Chem. A*, 2015, **3**, 18229-18237.
- [36] D. Li, L.-X. Ding, H. Chen, S. Wang, Z. Li, M. Zhu and H. Wang, *J. Mater. Chem. A*, 2014, **2**, 16617-16622.
- [37] K. Ai, Y. Liu, C. Ruan, L. Lu and G. Lu, *Adv. Mater.*, 2013, **25**, 998-1003.
- [38] J. W. F. To, Z. Chen, H. Yao, J. He, K. Kim, H.-H. Chou, L. Pan, J. Wilcox, Y. Cui and Z. Bao, *ACS Cent. Sci.*, 2015, **1**, 68-76.

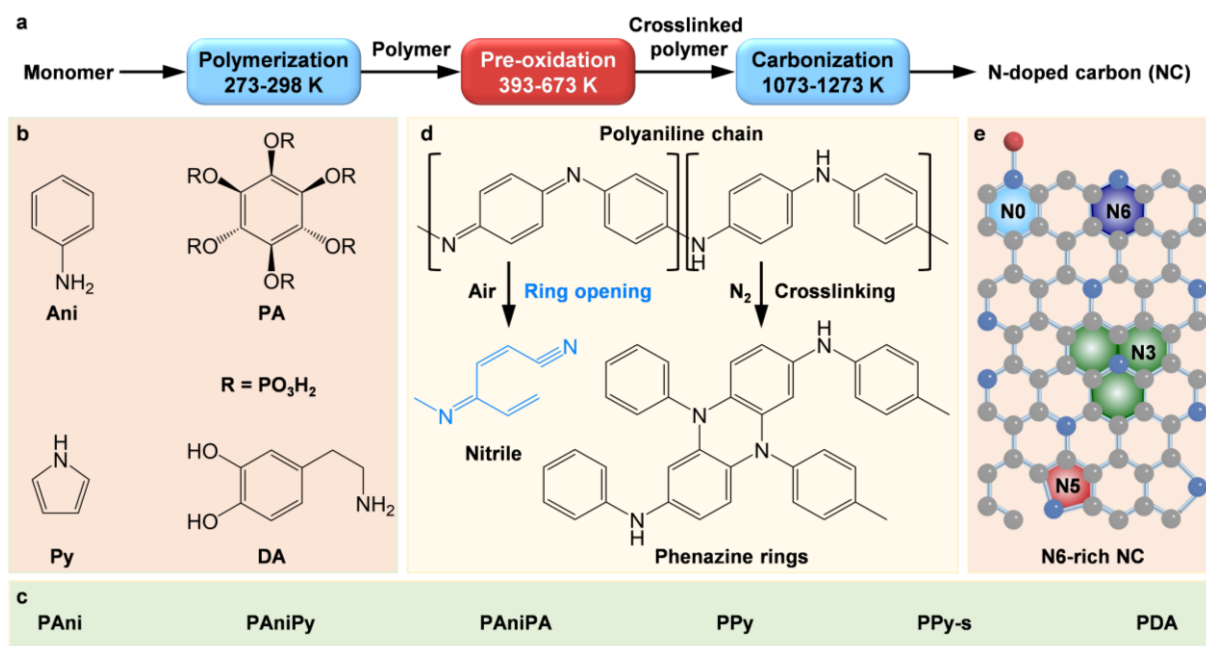


**Figure 1.** (a) Synthetic strategy towards highly nitrogen-doped carbons (e), comprising the polymerization of different monomers (b), followed by controlled peroxidation, and carbonization of the corresponding polymers (c). The peroxidation treatment has prominent influence on the development of different nitrogen functionalities of crosslinked polymers as exemplified with polyaniline (d). Monomer: aniline (An), pyrrole (Py), phytic acid (PA), dopamine (DA). (Co)Polymers: polyaniline (PAni), polyaniline-polypyrrole (PAniPy), polyaniline-phytic acid (PAniPA), polypyrroles (PPy, PPy-s), polydopamine (PDA). Nitrogen speciation in NC: N6: pyridinic N, N5: pyrrolic N, N3: quaternary N, N0: oxidized pyridinic N.

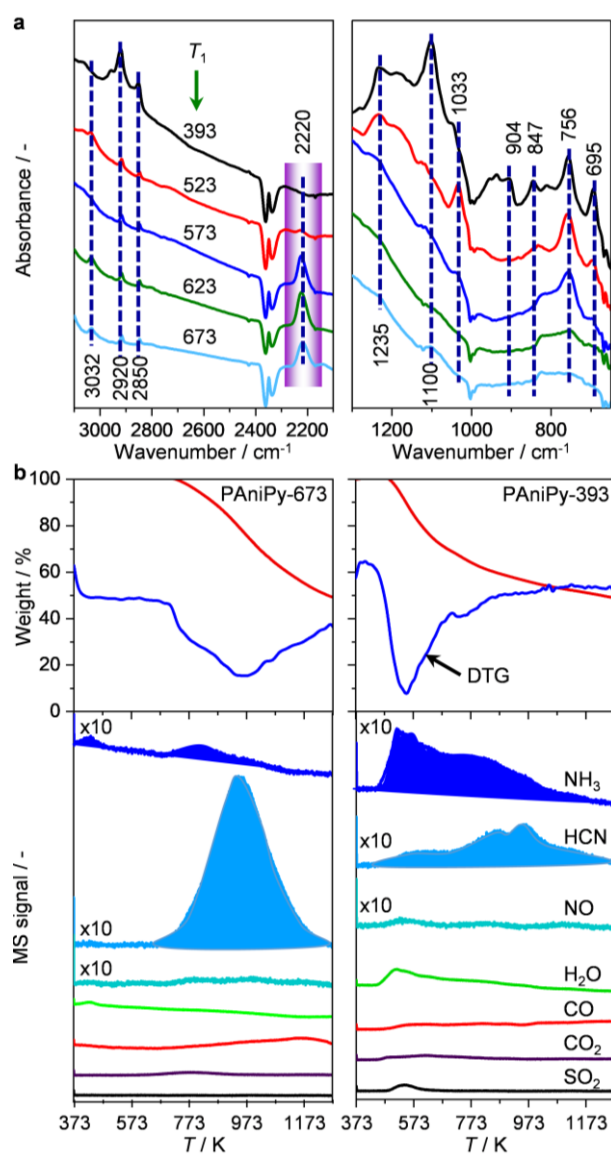


**Figure 2.** (a) *Ex situ* DRIFT spectra of PANiPy polymers after pre-oxidizing at different temperatures ( $T_1$ ), and (b) the representative TG/DTG profiles in Ar accompanied with corresponding MS signals of various fragments.

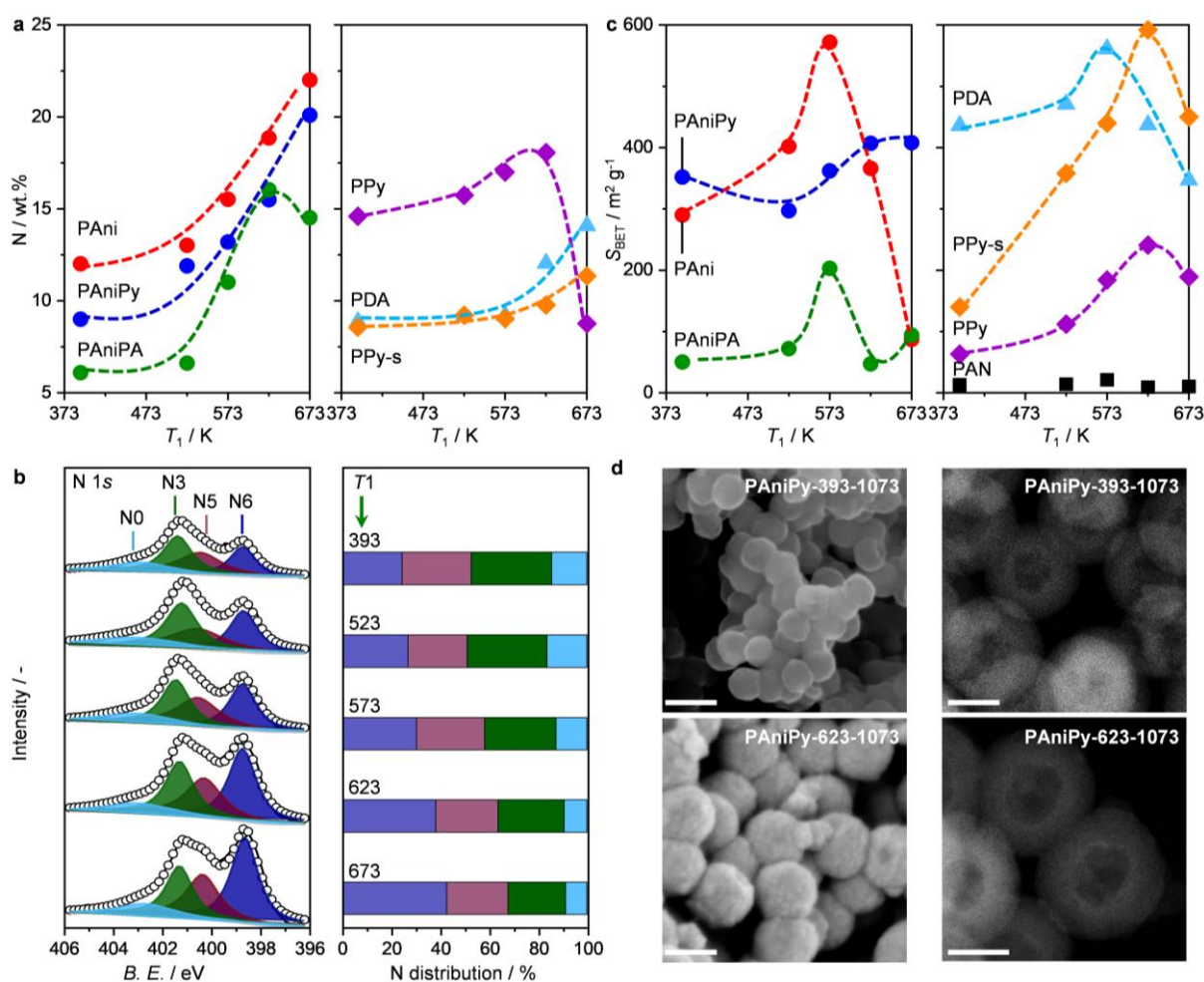


**Figure 3.** Characterization of N-doped carbons derived from different polymer precursors. The total nitrogen content (**a**), determined by the elemental analysis, and the specific surface area ( $S_{BET}$ , **b**), determined by N<sub>2</sub> sorption, as a function of the pre-oxidation temperature for polyaniline-based and the rest (co)polymers. (**c**) The deconvoluted N 1s XPS spectra of N-doped carbons derived from the PANiPy- $T_1$  series, accompanied with the distribution of different nitrogen speciation. (**d**) HAADF-STEM images of selected N-doped carbons derived from the PANiPy polymers. Scale bars: 100 nm.

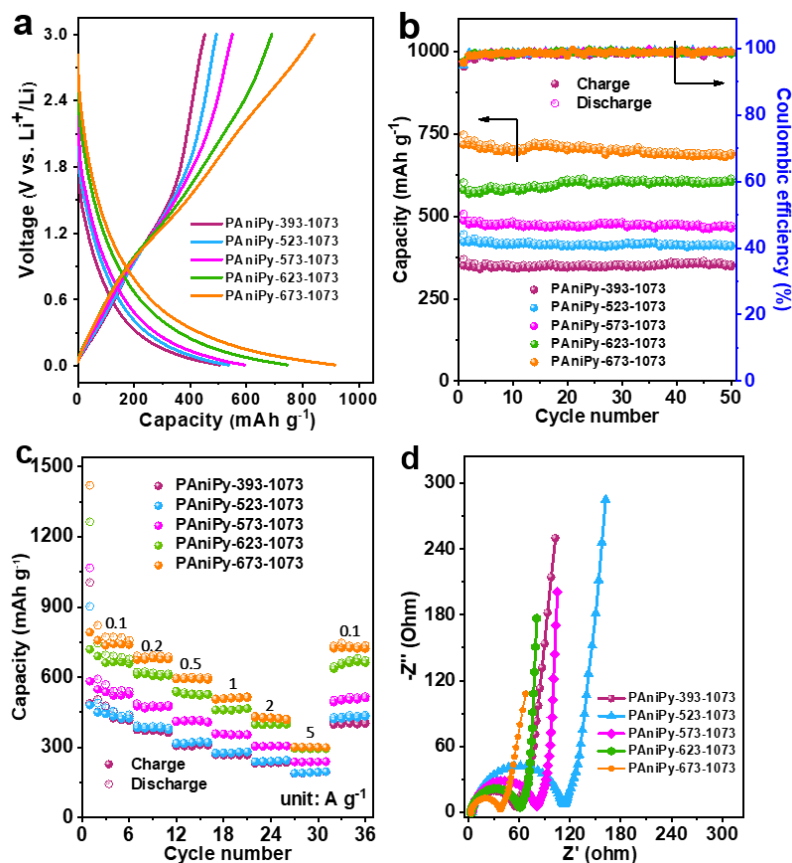


**Figure 4.** Electrochemical performance of PANiPy-*T*<sub>1</sub>-1073 as anode for LIBs in LiPF<sub>6</sub> electrolyte in the potential of 0.01 to 3.0 V vs. Li<sup>+</sup>/Li. **(a)** GCD profiles measured at 0.1 A g<sup>-1</sup>. **(b)** Cycling performance tested at 0.2 A g<sup>-1</sup>. **(c)** Rate capability recorded at different current densities from 0.1 to 5 A g<sup>-1</sup>. **(d)** EIS profiles.

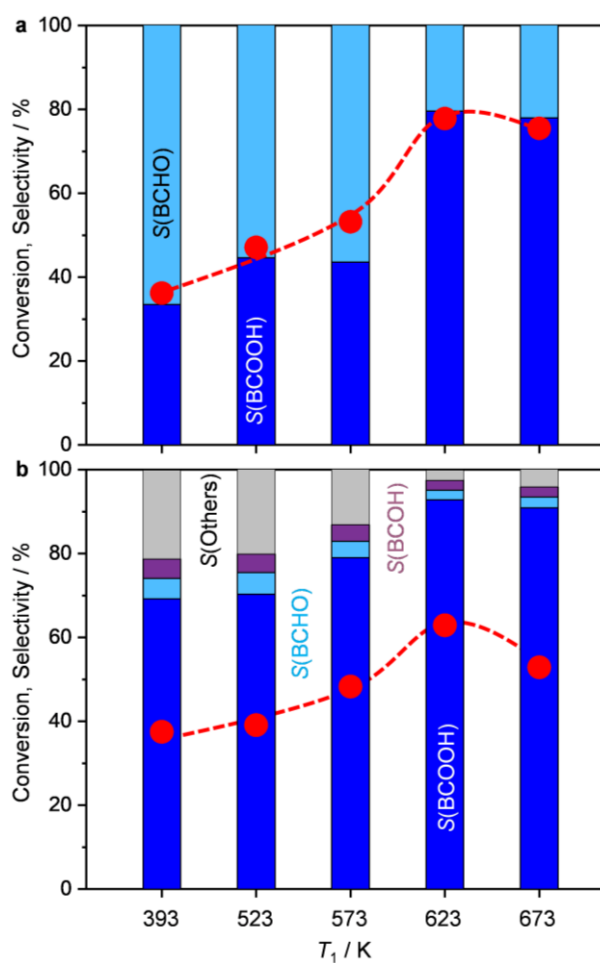


**Figure 5.** Catalytic performance of PAniPy- $T_1$ -1073 in the selective oxidation of (a) benzyl alcohol (BCOH) and (b) toluene. Reaction conditions: substrate, 1 mmol,  $H_2O$ , 3 cm<sup>3</sup>, TBHP (70 wt.% in  $H_2O$ ), 0.5 cm<sup>3</sup>, catalyst, 10 mg,  $T = 373$  K and  $t = 6$  h. Conversion and selectivity are indicated by the circles and bars, respectively. BCHO, benzaldehyde; benzoic acid, BCOOH.

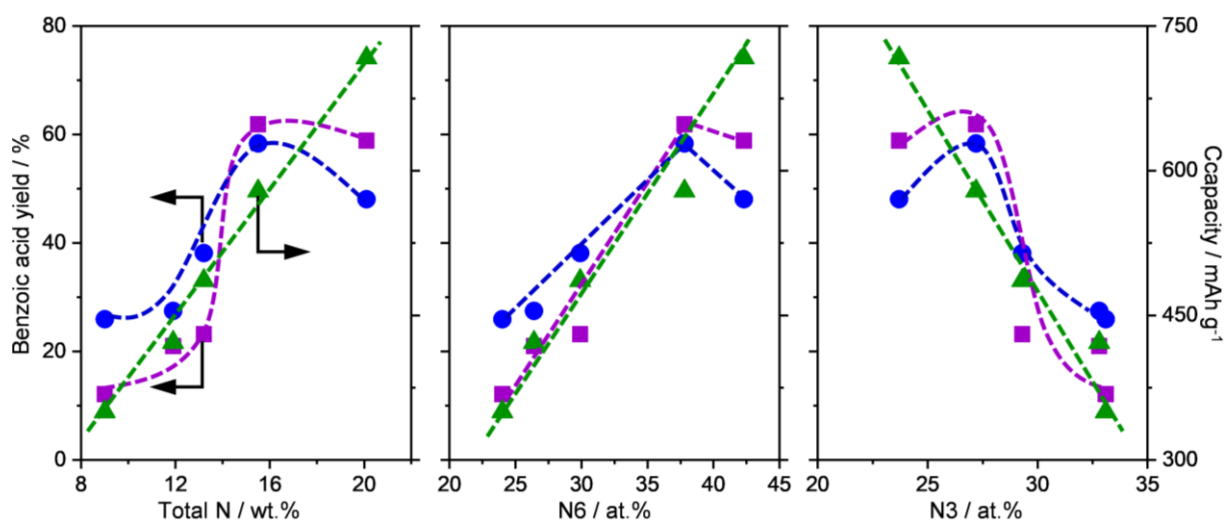


**Figure 6.** Correlations of the catalytic and electrochemical performances of the PAniPy-T<sub>1</sub>-1073 series as a function of the total nitrogen and the shares of N6 and N3 speciation. The yield of benzoic acid was used as the activity descriptor in benzyl alcohol (squares) and toluene (circles) oxidation, while the capacity of charge at the first cycle tested at 0.2 A g<sup>-1</sup> was taken. The dashed lines are for purpose of eye guide.

**Highly** doped carbons with rich pyridinic nitrogen speciation are facilely fabricated by a general approach coupling controlled pre-oxidation and subsequent carbonization of various N-bearing (co)polymers; these novel materials can afford remarkable catalytic performance in the selective oxidation of diverse substrates and outstanding capacity and cycling performance in lithium ion batteries.

**Keywords:** polymer, nitrogen-doped carbon, synthetic strategy, catalysis, lithium ion battery

Xiaoling Mou, Jiaxin Ma, Shuanghao Zheng, Xingkun Chen, Frank Krumeich, Roland Hauert, Ronghe Lin,\* Zhong-Shuai Wu,\* and Yunjie Ding\*

### A General Synthetic Strategy Towards Highly Doped Pyridinic Nitrogen-Rich Carbons

